Struct Chem (2017) 28:1501–1511
DOI 10.1007/s11224-017-0982-3

ORIGINAL RESEARCH

Exploring the substrate selectivity of human sEH and *M. tuberculosis* EHB using QM/MM

Sandra Rabi[1] · **Anand H. G. Patel**[1] · **Steven K. Burger**[1] · **Toon Verstraelen**[2] · **Paul W. Ayers**[1]

Received: 11 March 2017 / Accepted: 24 May 2017 / Published online: 9 June 2017

Abstract The mechanisms of human soluble epoxide hydrolase (sEH) and the corresponding epoxide hydrolase enzyme from *Mycobacterium tuberculosis* (EHB) are studied computationally, using the quantum mechanics/molecular mechanics (QM/MM) method. To do this, we modeled the alkylation and the hydrolysis steps of three substrates: *trans*-1,3-diphenylpropene oxide, *trans*-stilbene oxide and *cis*-stilbene oxide. Studying the regioselectivity for *trans*-1,3-diphenylpropene oxide, we determined that both enzymes prefer ring opening via attack on the benzylic carbon. In agreement with experimental studies, our computations show that the rate-limiting step is hydrolysis of the ester intermediate, with reaction barriers of approximately 13 to 18 kcal/mol. Using the barrier energies of this rate-limiting step, the three epoxides were ranked in order of reactivity. Though the reactivity order was correctly predicted for sEH, the predicted order for EHB did not correspond to experimental observations. Next, the electrostatic contributions of individual residues on the barrier height of the rate-limiting step were also studied. This revealed several residues important for catalysis. The secondary tritium kinetic isotope effect for the alkylation step was determined using a cluster model for the active site of sEH. The calculated value was 1.27, suggesting a late transition state for the rate-limiting step. Finally, we analyzed the reactivity trends using reactivity indicators from conceptual density functional theory, allowing us to identify ease of electron transfer as the primary driving force for the reaction.

Keywords Epoxide hydrolase mechanism · QM/MM · Tuberculosis antibiotics · sEH · Epoxide hydrolase B

Introduction

Tuberculosis (TB) infections account for one of the top 10 causes of death worldwide [1], with a staggering 1.5 million deaths reported in 2014 alone [2]. Development of antibiotics to treat *Mycobacterium tuberculosis* (MTB), the bacterium that causes TB [1], has been challenging due to the constant evolution of new antibiotic resistant MTB strains [3]. Though bacterial antibiotic resistance is often conferred through many pathways, one resistance pathway in MTB may be mediated via epoxide hydrolase (EH) enzymes. These enzymes generally convert epoxides to diols, and are important for neutralizing toxic compounds in an organism [4]. In the MTB genome, 30 different EH enzymes have been potentially identified, a relatively high number that alludes to the importance of these enzymes for the organism's survival [5].

Of the many EHs that MTB can code for, certain EHs may be important drug targets [5]. This suggestion comes from a previous genomic study on the model organism, *Mycobacterium marinum* (MTM), which identified mel_2, a conserved locus between MTM and MTB [6]. Mutations on this locus cause MTM to lose the ability to infect murine and fish macrophage cells. In MTB, mel_2 contains the following genes: Rv1936, Rv1937, Rv1938, Rv1939, Rv1940, and Rv1941. Due to the large number of EHs found in the MTB genome, Rv1983, which codes for EHB [6], was proposed to be a potential drug target [5].

However, the production of EH enzymes is not limited to MTB; many organisms, including humans, also use these

This paper is dedicated to Professor Lou Massa on the occasion of his Festschrift.

✉ Anand H. G. Patel
patela69@mcmaster.ca

[1] Department of Chemistry and Chemical Biology, McMaster University, 1280 Main St. W, Hamilton, Ontario L8S 4M1, Canada

[2] Center for Molecular Modeling, Ghent University, Technologiepark 903, 9052 Zwijnaarde, Belgium

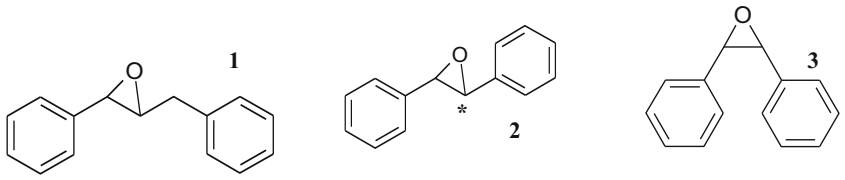

Fig. 1 The three substrates considered in this study: (*1*) *trans*-1,3-diphenylpropene oxide, (*2*) *trans*-stilbene oxide, and (*3*) *cis*-stilbene oxide

enzymes for many purposes [4]. An important human EH is soluble epoxide hydrolase (sEH), mainly found in the cytosol of hepatocytes [7]. The C-terminal domain of this enzyme shares structural similarities with EHB [5] (Fig. 3), suggesting that both enzymes might share specificity for particular ligands. This is supported by an experimental study that tested the specific activity of EHB for three substrates (Fig. 1): *trans*-1,3-diphenyl propene oxide, *trans*-stilbene oxide, and *cis*-stilbene oxide [5]. Similar to human sEH, EHB was approximately 10 times more active for *trans*-1,3-diphenyl propene oxide than for *trans*-stilbene oxide. This shared specificity implies that care must be taken to ensure that a drug designed to inhibit EHB does not also bind to human sEH, which may cause unwanted side effects. Thus, this study aims to compare the mechanisms of human sEH and EHB for three substrates (Fig. 1), to further understand the factors driving their substrate specificities.

As expected from their structural similarities, human sEH and EHB both follow the general EH mechanism [8] (Fig. 2). The key residues involved in this mechanism include several Tyr residues involved in stabilizing the substrate via hydrogen bonding [9], and an Asp-His-Asp catalytic triad [8]. In the first step, one of the nucleophilic Asp residues alkylates an epoxide carbon [8]. Next, the covalent intermediate is hydrolyzed using the His residue as a proton acceptor. This hydrolysis forms the diol product, and is the rate-limiting step in the overall reaction [10].

In addition to several experimental studies of this mechanism [8, 9, 11, 12], a number of theoretical studies have been done on the mechanism of sEH [13–16]. These studies can

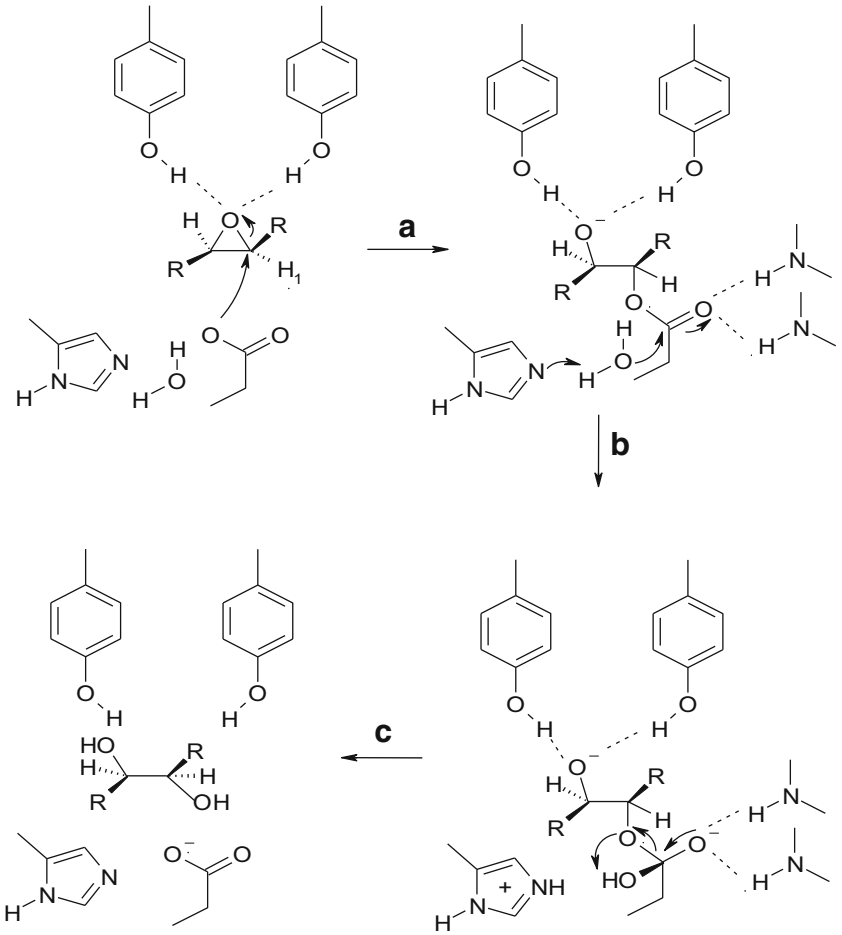

Fig. 2 An overview of the generally accepted mechanism for epoxide hydrolase. **a** One of the epoxide carbons is attacked by a nucleophilic Asp residue to form a covalent enzyme-substrate complex. **b** The His residue acts as a base to abstract a proton from water; the resulting hydroxide forms a tetrahedral intermediate that is hydrolyzed in (**c**)

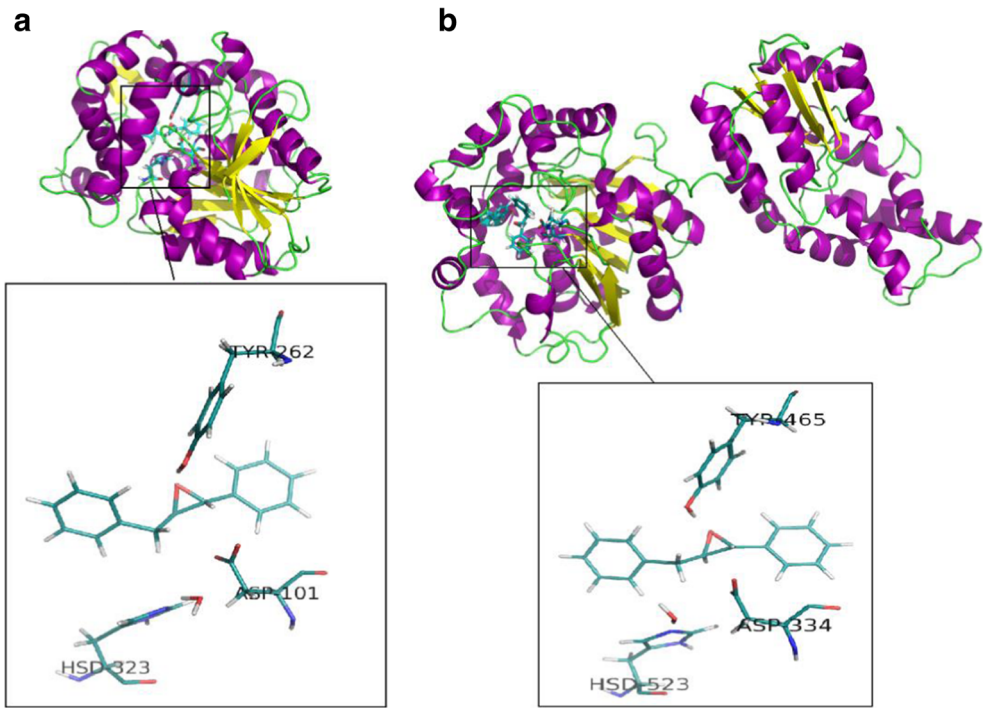

Fig. 3 **a** Structure of MTB epoxide hydrolase B (PDB entry 2E3J) [5] and the QM subsystem. **b** Equivalent representation for human soluble epoxide hydrolase (PDB entry 1S8O) [36]. From the structures of both enzymes, the similarities between the C-terminal domain of human epoxide hydrolase and epoxide hydrolase B can be observed

broadly be classified as either quantum mechanics (QM) or molecular dynamics (MD) based. The earliest QM study used a small model system to study the mechanism of EH [13]. Due to the relatively high cost of QM methods, the model system consisted of an acetic acid molecule attacking the epoxide. Despite a truncated model system, this study was able to observe the role of surrounding Tyr residues in reducing the energy barrier for epoxide ring opening. A more recent QM study used a larger cluster model based on the X-ray structure of human sEH [14]. The model in this study consisted of a catalytic water, and seven residues from the active site, including a catalytic aspartate, catalytic histidine, and the two tyrosine residues. (1S,2S)-β-Methylstyrene oxide (MSO) was used a substrate for the reaction. Both alkylation and hydrolysis were investigated along with the regioselectivity of the epoxide opening. However, the large size of the cluster led to geometry optimization issues, with multiple minima being observed. This suggests that a less rigorous model, such as MD, may be more suited to simulate systems of this size. In particular, a study on murine sEH was done using MD to study the formation of near attack conformations for the first step of the EH mechanism [16]. It was found that hydrogen bonding between the catalytic histidine and the catalytic aspartate might be important to allow effective catalysis.

Though QM and MD approaches have been valuable in furthering the understanding of the EH mechanism, they also have disadvantages. Though rigorous, QM approaches are also quite expensive, limiting the system size that can be simulated. Contrary to the QM approach, MD approaches are cheap, but may not give an accurate picture of a chemical reaction. A blend of both of these approaches, quantum mechanics/molecular mechanics (QM/MM) [17–25], minimizes these drawbacks of using either QM or MD, since the reaction site of an enzyme can be modeled using QM, while the rest can be included using MM. Thus, in this study, we propose using a QM/MM-based approach to studying the mechanisms of sEH and EHB.

The QM/MM approach will be used to study the mechanism from several perspectives. The first will be to determine the regioselectivity of sEH and EHB for substrate 1, in order to determine if a difference exists between the two enzymes. This will be done through comparing the transition state (TS) energies of the rate-limiting step for ring opening on either epoxide carbon. Next, the catalytic rates of EHB and sEH will be compared for substrates 1–3. This will also be done using computed TS energies for the rate-limiting step. Third, a charge mutation analysis [26–28] will be conducted for the catalysis of substrate 1. By setting the charge of each residue to zero and observing the change in TS energies for the rate-limiting step, the stabilizing or destabilizing effects of residue charge can be assessed. Further insight into the nature of the TS of the rate-limiting step is gained by determining the secondary kinetic isotope effect (KIE) for the catalysis of substrate 2 by human sEH will be determined. Finally, we use reactivity indicators from conceptual density functional theory [29–35] to identify the physical effects that are responsible for the reactivity preferences we have observed. Through these investigations, we aim to further the understanding of the mechanistic differences between sEH and EHB. This understanding can then be used to aid in designing TB therapeutics that selectively target EHB.

Computational methods

System setup and MD simulations

The initial structures were taken from the crystal structures of MTB EHB (PDB entry 2E3J [5], Fig. 3a) and human sEH (PDB entry 1S8O [36], Fig. 3b). Hydrogen atoms were added using MolProbity [37]. All molecular dynamics calculations were done using Sigma v.2.2 [38] with the CHARMM22 force field [39]. The three substrates (Fig. 1) were optimized in the gas phase and manually docked into the active site of each enzyme, giving a total of six different ligand-enzyme complexes. To ensure that the tested substrates were docked in reasonably correct orientations, the original inhibitor-bound crystal structures were used as a visual template. To equilibrate the system, 20 ps of MD was performed as an initial relaxation step to remove steric hindrance between atoms in the initial docked structure. This was followed by 40 ps of MD. During the MD calculation, the backbone of the enzyme was constrained, and a cutoff of 12 Å was used. All of the parameters, with exception of the charges, were adapted from a previous work on *trans*-methylstyrene oxide [16].

QM/MM calculations

QM/MM calculations were done on the resulting MD structures, using Sigma [38] interfaced to Gaussian03, revision C.02 [40]. The QM/MM boundary was described with pseudobonds, which involves replacing the MM atoms bonded to QM atoms with parameterized pseudopotentials [41]. Structures for the stationary points were initially optimized with HF/3-21G [42–47], followed by B3LYP [48–51]/6-31G* [52]. The QM system included the substrate, the aspartate side chain (Asp104 for MTB EHB, and Asp334 for human sEH), the imidazole ring of histidine (His323 for MTB EHB, and His523 for human sEH), a conserved crystal water, and the side chain of one of the tyrosine residues (Tyr262 for MTB EHB, and Tyr465 for human sEH) that was predicted to be responsible for the hydrogen transfer to the ester intermediate.

Transition state calculations

The transition states (TSs) were initially located on a reduced 2 dimensional energy surface, and then refined using the standard TS optimizer in g03 [40]. For the first mechanistic step, the two variables to form the reduced surface include: (1) the distance between an epoxide carbon and the nucleophilic oxygen on the catalytic Asp, and (2) the distance between the same epoxide carbon and the bridging epoxide oxygen. For the second step, the reduced surface consisted of: (1) the distance between the carbonyl carbon of the catalytic aspartate and the oxygen of the water, and (2) the distance between the catalytic histidine nitrogen and one of the water protons. On both these reduced potential energy surfaces, a coarse scan was initially done to get an estimate of the TS location. This was followed by a Bofill update TS search on the reduced surface [53].

Residue analysis

The influence of residues in the MM region on the energy barrier of the rate-limiting step, hydrolysis of the ester intermediate, was studied by means of a charge deletion analysis [26–28]. This involved doing single point energy calculations for the reactant and TS structure with all the charges on a particular residue set to zero. This analysis was done on all residues within 15 Å of the substrate (211 residues for MTB EHB and 188 residues for human sEH).

Kinetic isotope effect

To calculate the kinetic isotope effect (KIE) of the catalysis of substrate 2 by human sEH, the enzyme active site was taken and capped with hydrogen atoms to form a gas-phase cluster. The cluster model had the substrate, part of the catalytic aspartate, both of the tyrosine residues, and the conserved crystal water. The structures were optimized and frequency calculations were done using B3LYP [48–51]/6-31G* [52]. The transition state was calculated using the *Gaussian* TS search algorithm. Based on the partition function secondary tritium KIE for the alkylation step (the substituted hydrogen is marked * in Fig. 1) was calculated using the TAMkin package [54]. Tunneling corrections were applied according to Miller's formula [55].

Conceptual density functional theory analysis

We evaluated condensed reactivity indicators associated with conceptual density functional theory using the response of molecular fragment approach and atomic populations computed with natural population analysis [56, 57]. This required performing B3LYP/6-31G* calculations, using geometries optimized by the procedure described in *2.2*, for the system with one additional electron and with one less electron. Using the atomic charges from these calculations, we computed and analyzed the condensed Fukui function [58, 59] and condensed dual descriptor [60–63] for key atoms at key points along the reaction pathway. We also investigated whether the reactivity preferences followed the trends that would be expected from the maximum hardness principle [64–66] but in this case, perhaps unsurprisingly [67–69], the maximum hardness principle seems to be a poor predictor of reactivity preferences.

Results and discussion

Optimization and comparison of the catalytic mechanisms

To confirm that both MTB EHB and human sEH follow the same general mechanism, the mechanisms of both enzymes were compared for substrates 1–3. As expected, it was found that the optimized structures were almost identical for both of the enzymes, with a RMSD of less than 0.1 Å. Additionally, for both the alkylation and hydrolysis steps, the overall geometries of the TS and intermediates were compared to a previous theoretical study on human sEH [14]. This ensured that the parameters and QM/MM boundary chosen for the calculations are appropriate for the remainder of this study.

To initiate the alkylation step, the catalytic aspartate (Asp334 for human sEH and Asp101 for MTB EHB) is observed to be in the correct position to attack the epoxide ring on the substrates. This was observed to occur in concert with a proton transfer to the epoxide oxygen from a nearby Tyr residue (Tyr 465 in human sEH and Tyr 262 in EHB) to form an ester intermediate. The observations for the nucleophilic aspartate positioning are in agreement with previous work [14]. However, the concerted proton transfer observed from the Tyr465/262 residue does not agree with the previous study on human sEH [14]. This previous work found that the protonation of the epoxide oxygen occurs after the alkylation by Asp334/101, rather than in a concerted fashion. Thus, to determine if a separate protonation step could be replicated, a deprotonated intermediate was optimized with two nearby Tyr residues protonated. However, the proton from Tyr465/262 was found to automatically transfer to the intermediate. This indicates that a deprotonated intermediate may not be stable, and that the protonation occurs alongside the alkylation step.

Once the ester intermediate is produced, the catalytic histidine (His523 in human sEH and His323 in MTB EHB) abstracts a proton from a water molecule, with the resulting hydroxyl added to the ester. This is in agreement with experimental studies for *Agrobacterium radiobacter* AD1 EH [8], potato RH [70], and microsomal EH [71]. Comparing the TS energy of the hydrolysis step to that of the alkylation step confirms that hydrolysis is the rate-limiting step. Overall, observations for the two steps seem to be in good agreement with those reported in the literature [13, 15], validating the calculations performed.

Studying the regioselectivity of the alkylation step

Once the overall mechanism was reproduced in good agreement with the literature, the regioselectivity of the reaction was tested for substrate 1. The energy of the alkylation and hydrolysis steps were computed for both epoxide carbons. The full energy curves for sEH are given in Fig. 4, and the corresponding curves for EHB are given in Fig. 5. For both figures, attack on the benzylic carbon has a lower energy barrier for the rate-limiting step when compared to attack on the homo-benzylic carbon. This observation is expected, as the benzylic carbon is generally more stabilized and electrophilic.

Comparison of enzymatic rates for varying substrates

Next, the effect of different ligands on the catalytic rate of the two enzymes was also explored. This was done by computing the transition state energies of the two steps for each ligand. The step with the highest energy, which is the rate-limiting step, can be used to determine the catalysis rates for each enzyme. For human sEH, the full TS energy curves for substrates 1–3 are given in Fig. 4, and for MTB EHB, the curves are given in Fig. 5. For all of the full energy curves in Figs. 4 and 5, experimental TS barrier energies were found using experimental values for the specific activities of each substrate [5, 72]. These specific activities were converted to the barrier energy of the rate-limiting step using TS theory [73].

Comparison of the experimental and calculated barriers for the rate-limiting hydrolysis step shows that the computed barriers consistently underestimate the overall barrier height. This is likely due to the use of DFT, which tends to underestimate barrier energies. Thus, a more quantitative assessment of the rates is not feasible using these calculated results. A more qualitative assessment of the relative substrate reactivity for human sEH shows that the experimental order [72] is reproduced by the calculation, with $1 > 2 > 3$. However, this is not the case for EHB, where the experimental order is $1 > 3 > 2$ [5], but the calculated order is $1 > 2 > 3$. These results suggest that the QM method chosen for this calculation may need to be more accurate to reproduce the appropriate order of substrate reactivity.

Charged residue analysis

To determine the stabilizing or destabilizing effects of charged residues on the mechanism of sEH and EHB, the charge on each residue was set to zero, and the change in barrier height ($\Delta\Delta E$) was observed [26–28]. The residue nomenclature used here is the human sEH residue number first, followed by the residue number of MTB EHB. The residues that showed a significant $\Delta\Delta E$ included: Glu269/38, Trp336/105, Asp496/292, and His334/103. Of these, charge removal on Glu269/38, Trp336/105, and Asp496/292 was found to have a positive $\Delta\Delta E$ value, corresponding to a destabilization of the rate-limiting TS (rTS). In contrast, His334/103 was found to have a negative $\Delta\Delta E$ value, corresponding to a stabilization of the rTS.

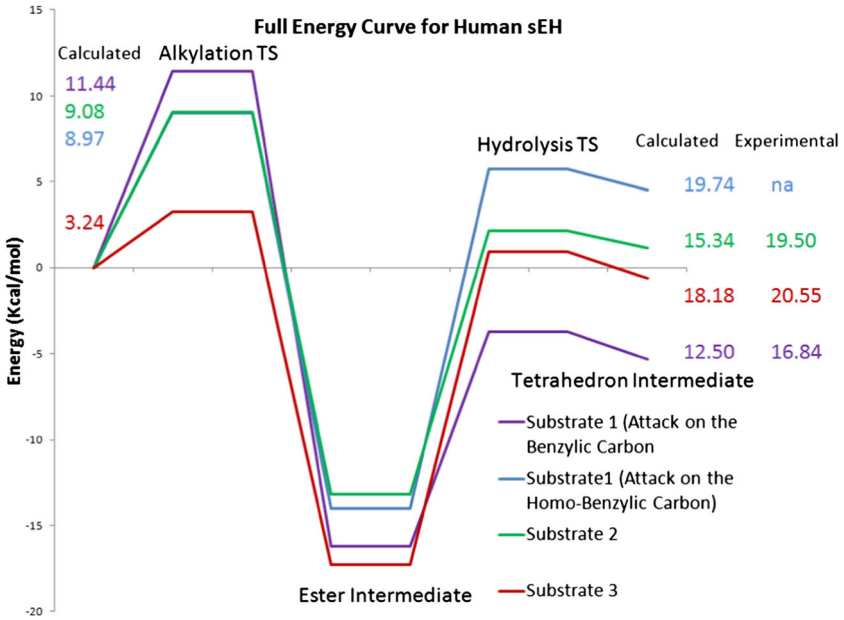

Fig. 4 Full energy curves for all the catalysis of all three substrates by human soluble epoxide hydrolase. Additionally, the regiochemistry for the substrate 1 reaction was tested using the energy curves for ring opening on either the benzylic carbon or homo-benzylic carbon

Glu269/38 Setting the charge of Glu269/38 to zero increases the rTS barrier by approximately 5–7 kcal/mol for both enzymes (Figs. 6 and 7). This suggests that the residue charge is important in the overall catalysis rate. This finding is corroborated by an experimental study that mutated the equivalent Glu residue in StEH1, a potato epoxide hydrolase [74]. This study mutated the carboxylate of this residue to an amide, which decreased the overall k_{cat} 40-fold for (R,R)-*trans*-stilbene oxide. From this, it was suggested that the Glu residue plays a part in activating the nucleophilic Asp, along with modulating the acid-base character of the catalytic histidine. This is likely the role of the conserved Glu269/38 residues in sEH and EHB as well.

Trp336/105 By setting the charge of Trp to zero, the overall rTS barrier was increased by approximately 12 kcal/mol for both enzymes (Figs. 6 and 7). This dramatic destabilization of the rTS suggests that the Trp residue is vital for efficient catalysis. This is supported by the high degree of conservation of this Trp residue in many EHs [75]. It has been suggested that the Trp residue stabilizes the tetrahedral intermediate (step B, Fig. 2) in microsomal EH by hydrogen bonding to the oxyanion [71]. However, an experimental study on murine sEH found that mutation of the equivalent Trp residue to Phe did not significantly alter enzymatic activity towards *trans*-stilbene oxide [76]. In light of these findings, Trp was proposed to be important for substrate binding, but not

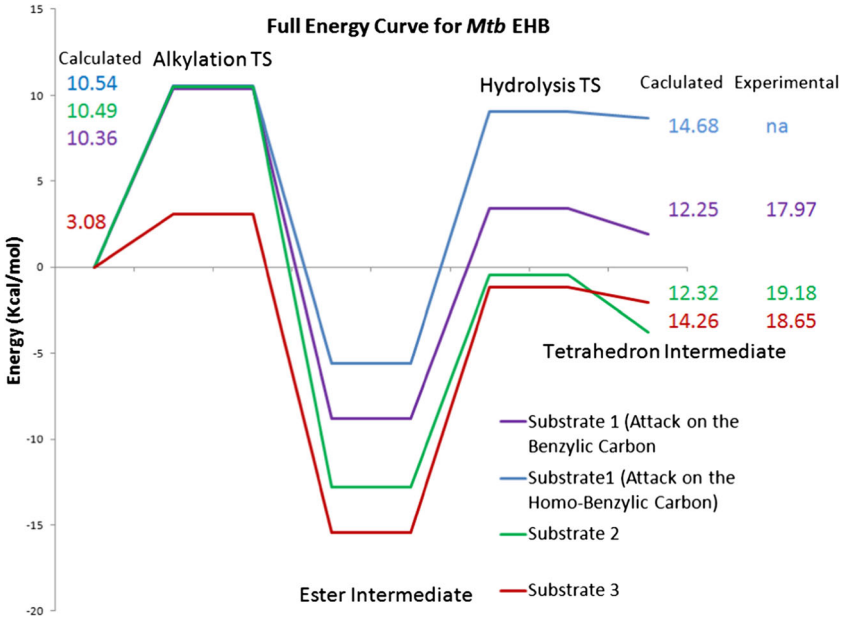

Fig. 5 Full energy curves for all the catalysis of all three substrates by MTB epoxide hydrolase B. Additionally, the regiochemistry for the substrate 1 reaction was tested using the energy curves for ring opening on either the benzylic carbon or homo-benzylic carbon

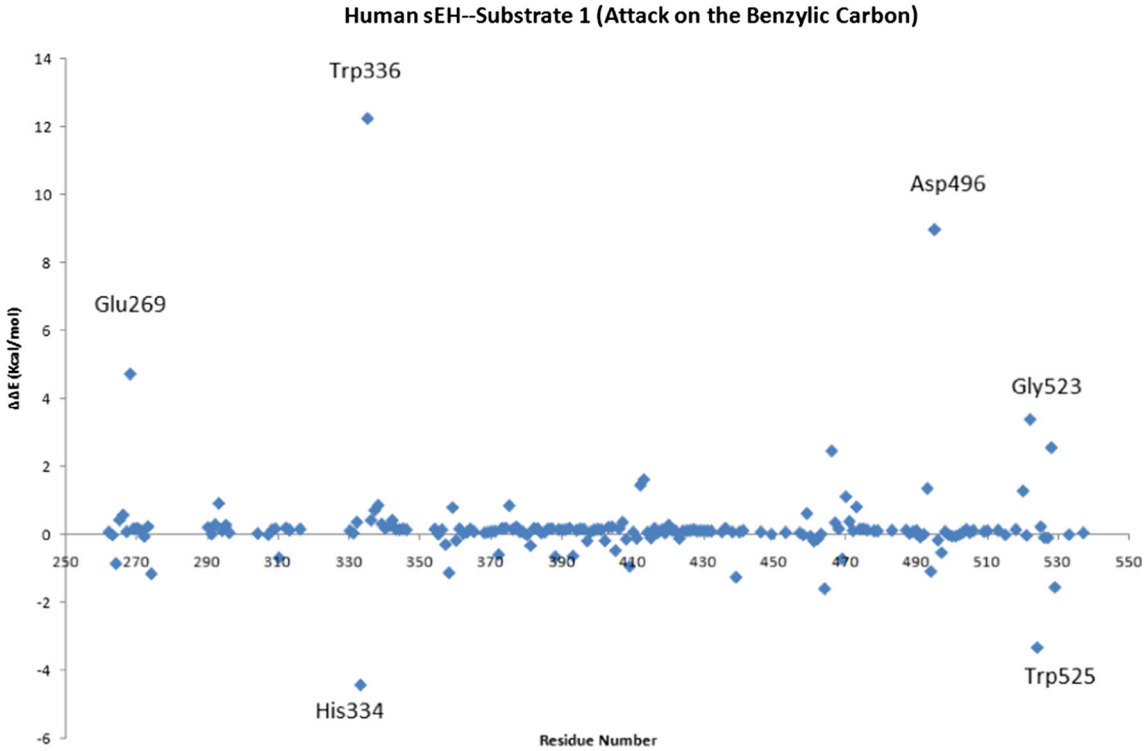

Fig. 6 Residue analysis for residues within 15 Å of substrate 1 in human soluble epoxide hydrolase. The change in rate-limiting step barrier is denoted ΔΔE (kJ/mol). This value is obtained from setting the charge on a given residue number to zero

involved mechanistically. For both enzymes in this study, human sEH and MTB EHB, this may also be the case.

Asp496/292 This residue is part of the Asp-His-Asp catalytic triad [8]. This Asp is thought to play an important role in

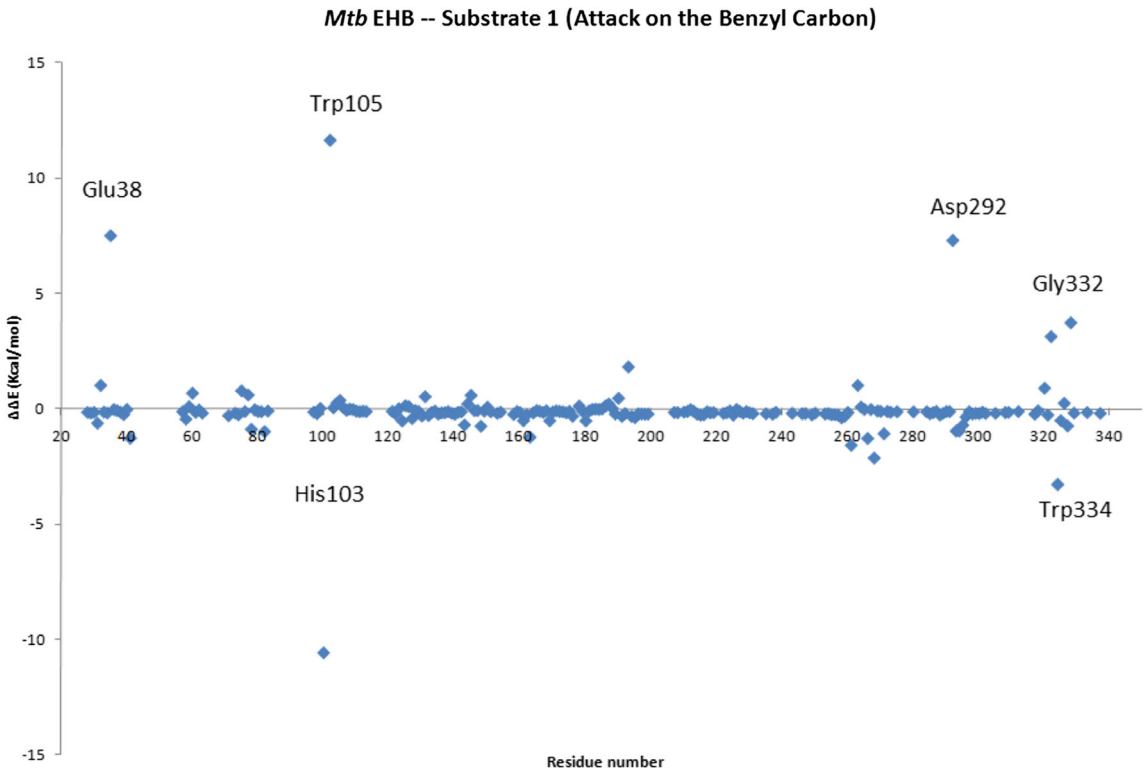

Fig. 7 Residue analysis for residues within 15 Å of substrate 1 in MTB epoxide hydrolase B. The change in rate-limiting step barrier is denoted ΔΔE (kJ/mol). This value is obtained from setting the charge on a given residue number to zero

orienting, and activating the nucleophilic Asp residue [4]. By setting the charge on this Asp to zero, the rTS barrier is increased by 7–9 kcal/mol for both enzymes (Figs. 6 and 7). Experimentally, mutation of this Asp residue in murine sEH led to a complete loss of enzymatic activity [76]. This experimental finding agrees well with the increase in rTS barrier height observed.

His334/103 Charge removal on this residue decreased the rTS barrier by approximately 4 and 11 kcal/mol for human sEH and MTB EHB, respectively. This suggests that the residue plays an important role in catalysis. However, its large distance from the active site makes it unlikely that the residue plays a direct role in substrate catalysis. In this case, it may be that is the residue plays a role in maintaining the overall structure of the enzyme. To confirm this, a mutagenesis study can be done, where MD simulations of the mutated enzyme are compared to that of the wild type. Additionally, to our knowledge, no experimental studies have been done for this residue, or its analogues, in sEH, EHB or any other EH enzymes. Thus, future studies elucidating the role of this residue may be needed.

Kinetic isotope effect of sEH

The secondary KIE of substrate 2 was computed by substituting the hydrogen in Fig. 1 marked by an * with tritium, and then running a frequency analysis. This produced a calculated secondary KIE effect of 1.271. A previous study on soybean EH also found a similar secondary KIE of 1.30 for the catalysis of 9,10-epoxystearate [77]. The interpretation given for this high KIE value is that the epoxide bond is broken prior to nucleophilic attack by the Asp residue. Given the similarities between the EH enzymes and their mechanisms, this suggests that a late TS may also be the case for human sEH.

Conceptual DFT analysis

We analyzed the atomic charges, condensed Fukui functions, and condensed dual descriptor at different points of the reaction coordinate. Based on our analysis, the key difference between the substrates is the susceptibility of the aspartate carbon to nucleophilic attack by the water oxygen (cf. step b of Fig. 2). We then analyzed whether this increased susceptibility was likely to be due to electrostatic effects (more positively charged carbon atoms will be more reactive) or electron transfer (carbon atoms with higher values of the condensed dual descriptor will be more electrophilic). As seen in Table 1, only the dual descriptor captures the experimentally observed reactivity trends. This suggests that the reactive rate of EH is, at least for these substrates, modulated primarily by the ability of the aspartate carbon to accept electrons in the ester intermediate.

Table 1 Atomic charges and condensed dual descriptor values for the aspartate carbon in the ester intermediate for human sEH and MTB EHB

Substrate	Atomic charge	Dual descriptor	Empirical reactivity
Human sEH			
1	0.863	0.149	Most
2	0.879	0.085	Intermediate
3	0.865	0.074	Least
MTB EHB			
1	0.881	0.181	Most
2	0.902	0.149	Least
3	0.895	0.179	Intermediate

The empirical reactivity order is consistent with the predictions of the dual descriptor

Conclusion

QM/MM has been used to study the reaction mechanisms of human sEH and MTB EHB from several perspectives. By simulating the alkylation and hydrolysis steps, it was confirmed that the two enzymes shared the same mechanism. We also showed that the proton transfer from Tyr likely occurs in a concerted fashion with the alkylation reaction, rather than in a separate step. Next, the regioselectivity of both enzymes for substrate 1 was tested. It was found that the benzylic position was preferred over the homo-benzylic position, for both enzymes. Once the regioselectivity of both enzymes was confirmed, the substrate preference for each enzyme was tested. We found that the QM/MM method produced qualitatively accurate results for sEH, but was unable to reproduce experimental results for EHB. To determine the residues with electrostatic effects important for the rate-limiting step, a charge analysis was conducted. This found several important residues for catalysis, including: Glu269/38, Trp336/105, Asp496/292, and His334/103. The secondary KIE for the catalysis of substrate 2 by human sEH was calculated to be 1.27, which suggests a late TS for the rate-limiting hydrolysis step. Finally, conceptual DFT analysis identifies the ability of the aspartate carbon in the ester intermediate to accept electrons as an important factor for determining the relative rate of reaction for different substrates.

Overall, these results fail to find any distinction between the mechanisms of EHB and sEH that may be useful for drug design. This suggests that facets of the mechanism other than those observed in this study need to be explored in future work. Additionally, the large impact on the rTS by His334/103 remains a mystery, and should also be studied further.

Acknowledgements The scientists dedicate this paper to Prof. Lou Massa. Lou was among the first people to show how analysis of the electron density can elucidate the features and reactivity of biomolecules, a perspective that informed and inspired the present work. The authors

thank the NSERC and the Canada Research Chairs program for funding, and Sharcnet and Compute Canada for computational resources.

Compliance with ethical standards

Conflict of interest The authors declare that they have no conflict of interest.

References

1. WHO (2016) WHO | Tuberculosis. In: WHO. http://www.who.int/mediacentre/factsheets/fs104/en/. Accessed 20 Feb 2017
2. WHO (2015) WHO Glocal tuberculosis report 2015. In: WHO. http://apps.who.int/iris/bitstream/10665/191102/1/9789241565059_eng.pdf. Accessed 20 Feb 2017
3. Georghiou SB, Magana M, Garfein RS, et al (2012) Evaluation of genetic mutations associated with Mycobacterium tuberculosis resistance to amikacin, kanamycin and capreomycin: a systematic review. PLoS One 7:e33275. doi:10.1371/journal.pone.0033275
4. Morisseau C, Hammock BD (2005) Epoxide hydrolases: mechanisms, inhibitor designs, and biological roles. Annu Rev Pharmacol Toxicol 45:311–333. doi:10.1146/annurev.pharmtox.45.120403.095920
5. Biswal BK, Morisseau C, Garen G, et al (2008) The molecular structure of epoxide hydrolase B from Mycobacterium tuberculosis and its complex with a urea-based inhibitor. J Mol Biol 381:897–912. doi:10.1016/j.jmb.2008.06.030
6. El-Etr SH, Subbian S, Cirillo SLG, Cirillo JD (2004) Identification of two *Mycobacterium marinum* loci that affect interactions with macrophages. Infect Immun 72:6902–6913. doi:10.1128/IAI.72.12.6902-6913.2004
7. Arand M, Grant DF, Beetham JK, et al (1994) Sequence similarity of mammalian epoxide hydrolases to the bacterial haloalkane dehalogenase and other related proteins. FEBS Lett 338:251–256. doi:10.1016/0014-5793(94)80278-5
8. Rink R, Fennema M, Smids M, et al (1997) Primary structure and catalytic mechanism of the epoxide hydrolase from agrobacterium radiobacter AD1. J Biol Chem 272:14650–14657. doi:10.1074/JBC.272.23.14650
9. Rink R, Kingma J, Lutje Spelberg JH, Janssen DB (2000) Tyrosine residues serve as proton donor in the catalytic mechanism of epoxide hydrolase from Agrobacterium radiobacter. Biochemistry 39:5600–5613. doi:10.1021/bi9922392
10. Laughlin LT, Tzeng HF, Lin S, Armstrong RN (1998) Mechanism of microsomal epoxide hydrolase. Semifunctional site-specific mutants affecting the alkylation. Half-reaction. Biochemistry 37:2897–2904. doi:10.1021/bi972737f
11. Borhan B, Jones AD, Pinot F, et al (1995) Mechanism of soluble epoxide hydrolase: formation of an alpha-hydroxy ester-enzyme intermediate through Asp-333. J Biol Chem 270:26923–26930. doi:10.1074/jbc.270.45.26923
12. Lacourciere GM, Armstrong RN (1993) The catalytic mechanism of microsomal epoxide hydrolase involves an ester intermediate. J Am Chem Soc 115:10466–10467. doi:10.1021/ja00075a115
13. Lau EY, Newby ZE, Bruice TC (2001) A theoretical examination of the acid-catalyzed and noncatalyzed ring-opening reaction of an oxirane by nucleophilic addition of acetate. Implications to epoxide hydrolases. J Am Chem Soc 123:3350–3357. doi:10.1021/ja0037724
14. Hopmann KH, Himo F (2006) Theoretical study of the full reaction mechanism of human soluble epoxide hydrolase. Chem - A Eur J 12:6898–6909. doi:10.1002/chem.200501519
15. Hopmann KH, Himo F (2006) Insights into the reaction mechanism of soluble epoxide hydrolase from theoretical active site mutants. J Phys Chem B 110:21299–21310. doi:10.1021/jp063830t
16. Schiøtt B, Bruice TC (2002) Reaction mechanism of soluble epoxide hydrolase: insights from molecular dynamics simulations. J Am Chem Soc 124:14558–14570. doi:10.1021/ja021021r
17. Warshel A, Levitt M (1976) Theoretical studies of enzymic reactions: dielectric, electrostatic and steric stabilization of the carbonium ion in the reaction of lysozyme. J Mol Biol 103:227–249
18. Senn HM, Thiel W (2009) QM/MM methods for biomolecular systems. Angew Chemie Int Ed 48:1198–1229. doi:10.1002/anie.200802019
19. Field MJ (2002) Simulating enzyme reactions: challenges and perspectives. J Comput Chem 23:48–58. doi:10.1002/jcc.1156
20. Field MJ, Bash PA, Karplus M (1990) A combined quantum mechanical and molecular mechanical potential for molecular dynamics simulations. J Comput Chem 11:700–733. doi:10.1002/jcc.540110605
21. Elber R, Karplus M (1987) A method for determining reaction paths in large molecules: application to myoglobin. Chem Phys Lett 139:375–380. doi:10.1016/0009-2614(87)80576-6
22. Warshel A, Weiss RM (1980) An empirical valence bond approach for comparing reactions in solutions and in enzymes. J Am Chem Soc 102:6218–6226. doi:10.1021/ja00540a008
23. Hu H, Yang W (2008) Free energies of chemical reactions in solution and in enzymes with ab initio quantum mechanics/molecular mechanics methods. Annu Rev Phys Chem 59:573–601. doi:10.1146/annurev.physchem.59.032607.093618
24. Karplus M (2014) Development of multiscale models for complex chemical systems: from H+H $_2$ to biomolecules (Nobel lecture). Angew Chemie Int Ed 53:9992–10005. doi:10.1002/anie.201403924
25. Warshel A (2014) Multiscale modeling of biological functions: from enzymes to molecular machines (Nobel lecture). Angew Chemie Int Ed 53:10020–10031. doi:10.1002/anie.201403689
26. Bash PA, Field MJ, Davenport RC, et al (1991) Computer simulation and analysis of the reaction pathway of triosephosphate isomerase. Biochemistry 30:5826–5832. doi:10.1021/BI00238A003
27. Mulholland AJ, Richards WG (1997) Acetyl-CoA enolization in citrate synthase: a quantum mechanical/molecular mechanical (QM/MM) study. Proteins Struct Funct Genet 27:9–25. doi:10.1002/(SICI)1097-0134(199701)27:1<9::AID-PROT3>3.0.CO;2-D
28. Wong KF, Watney JB, Hammes-Schiffer S (2004) Analysis of electrostatics and correlated motions for hydride transfer in dihydrofolate reductase. J Phys Chem B 108:12231–12241. doi:10.1021/jp048565v
29. Geerlings P, De Proft F, Langenaeker W (2003) Conceptual density functional theory. Chem Rev 103:1793–1873. doi:10.1021/cr990029p
30. Ayers PW, Anderson JSM, Bartolotti LJ (2005) Perturbative perspectives on the chemical reaction prediction problem. Int J Quantum Chem 101:520–534. doi:10.1002/qua.20307
31. De Proft F, Ayers PW, Geerlings P (2014) The conceptual density functional theory perspective of bonding. In: Frenking G, Shaik S (eds) The Chemical Bond. Wiley-VCH Verlag GmbH & Co. KGaA, Weinheim, Germany, pp 233–270
32. Johnson PA, Bartolotti LJ, Ayers PW et al (2011) Charge density and chemical reactions: a unified view from conceptual DFT. In: Gatti C, Macchi P (eds) Modern Charge-Density Analysis. Springer Netherlands, Dordrecht, pp 715–764
33. Gázquez JL (2008) Perspectives on the density functional theory of chemical reactivity. J Mex Chem Soc 52:3–10

34. Shu-Bin L (2009) Conceptual density functional theory and some recent developments. Acta Phys -Chim Sin 25:590–600. doi:10.3866/PKU.WHXB20090332
35. Roos G, Geerlings P, Messens J (2009) Enzymatic catalysis: the emerging role of conceptual density functional theory. J Phys Chem B 113:13465–13475. doi:10.1021/jp9034584
36. Gomez GA, Morisseau C, Hammock BD, Christianson DW (2004) Structure of human epoxide hydrolase reveals mechanistic inferences on bifunctional catalysis in epoxide and phosphate ester hydrolysis. Biochemistry 43:4716–4723. doi:10.1021/bi036189j
37. Chen VB, Arendall WB, Headd JJ, et al (2010) MolProbity: all-atom structure validation for macromolecular crystallography. Acta Crystallogr Sect D Biol Crystallogr 66:12–21. doi:10.1107/S0907444909042073
38. Mann G, Yun RH, Nyland L, et al (2002) The Sigma MD program and a generic interface applicable to multi-functional programs with complex, hierarchical command structure. In: Schlick T, Gan HH (eds) Comput. Methods Macromol. Challenges Appl. Springer, Berlin Heidelberg, pp. 129–145
39. MacKerell AD, Bashford D, Dunbrack RL, et al (1998) All-atom empirical potential for molecular modeling and dynamics studies of proteins. J Phys Chem B 102:3586–3616. doi:10.1021/jp973084f
40. Gaussian 03, Revision C.02, M. J. Frisch, G. W. Trucks, H. B. Schlegel, G. E. Scuseria, M. A. Robb, J. R. Cheeseman, J. A. Montgomery, Jr., T. Vreven, K. N. Kudin, J. C. Burant, J. M. Millam, S. S. Iyengar, J. Tomasi, V. Barone, B. Mennucci, M. Cossi, G. Scalmani, N. Rega, G. A. Petersson, H. Nakatsuji, M. Hada, M. Ehara, K. Toyota, R. Fukuda, J. Hasegawa, M. Ishida, T. Nakajima, Y. Honda, O. Kitao, H. Nakai, M. Klene, X. Li, J. E. Knox, H. P. Hratchian, J. B. Cross, V. Bakken, C. Adamo, J. Jaramillo, R. Gomperts, R. E. Stratmann, O. Yazyev, A. J. Austin, R. Cammi, C. Pomelli, J. W. Ochterski, P. Y. Ayala, K. Morokuma, G. A. Voth, P. Salvador, J. J. Dannenberg, V. G. Zakrzewski, S. Dapprich, A. D. Daniels, M. C. Strain, O. Farkas, D. K. Malick, A. D. Rabuck, K. Raghavachari, J. B. Foresman, J. V. Ortiz, Q. Cui, A. G. Baboul, S. Clifford, J. Cioslowski, B. B. Stefanov, G. Liu, A. Liashenko, P. Piskorz, I. Komaromi, R. L. Martin, D. J. Fox, T. Keith, M. A. Al-Laham, C. Y. Peng, A. Nanayakkara, M. Challacombe, P. M. W. Gill, B. Johnson, W. Chen, M. W. Wong, C. Gonzalez, and J. A. Pople (2004) Gaussian, Inc., Wallingford CT
41. Zhang YK, Lee TS, Yang W (1999) A pseudobond approach to combining quantum mechanical and molecular mechanical methods. J Chem Phys 110:46–54. doi:10.1063/1.478083
42. Binkley JS, Pople JA, Hehre WJ (1980) Self-consistent molecular orbital methods. 21. Small split-valence basis sets for first-row elements. J Am Chem Soc 102:939. doi:10.1021/ja00523a008
43. Dobbs KD, Hehre WJ (1987) Molecular orbital theory of the properties of inorganic and organometallic compounds. 6. Extended basis sets for second-row transition metals. J Comput Chem 8:880–893. doi:10.1002/jcc.540080615
44. Dobbs KD, Hehre WJ (1987) Molecular orbital theory of the properties of inorganic and organometallic compounds 5. Extended basis sets for first-row transition metals. J Comput Chem 8:861–879. doi:10.1002/jcc.540080614
45. Dobbs KD, Hehre WJ (1986) Molecular orbital theory of the properties of inorganic and organometallic compounds 4. Extended basis sets for third-and fourth-row, main-group elements. J Comput Chem 7:359–378. doi:10.1002/jcc.540070313
46. Pietro WJ, Francl MM, Hehre WJ, et al (1982) Self-consistent molecular orbital methods. 24. Supplemented small split-valence basis sets for second-row elements. J Am Chem Soc 104:5039–5048. doi:10.1021/ja00383a007
47. Gordon MS, Binkley JS, Pople JA, et al (1982) Self-consistent molecular-orbital methods. 22. Small split-valence basis sets for second-row elements. J Am Chem Soc 104:2797–2803. doi:10.1021/ja00374a017
48. Stephens PJ, Devlin FJ, Chabalowski CF, Frisch MJ (1994) Ab initio calculation of vibrational absorption and circular dichroism spectra using density functional force fields. J Phys Chem 98:11623–11627. doi:10.1021/j100096a001
49. Vosko SH, Wilk L, Nusair M (1980) Accurate spin-dependent electron liquid correlation energies for local spin density calculations: a critical analysis. Can J Phys 58:1200–1211. doi:10.1139/p80-159
50. Lee C, Yang W, Parr RG (1988) Development of the Colle-Salvetti correlation-energy formula into a functional of the electron density. Phys Rev B 37:785–789. doi:10.1103/PhysRevB.37.785
51. Becke AD (1993) Density-functional thermochemistry.III. The role of exact exchange. J Chem Phys 98:5648. doi:10.1063/1.464913
52. Rassolov VA, Ratner MA, Pople JA, et al (2001) 6-31G* basis set for third-row atoms. J Comput Chem 22:976–984. doi:10.1002/jcc.1058
53. Burger SK, Ayers PW (2010) Methods for finding transition states on reduced potential energy surfaces. J Chem Phys 132:234110. doi:10.1063/1.3445772
54. Ghysels A, Verstraelen T, Hemelsoet K, et al (2010) TAMkin: a versatile package for vibrational analysis and chemical kinetics. J Chem Inf Model 50:1736–1750. doi:10.1021/ci100099g
55. Miller WH (1974) Quantum mechanical transition state theory and a new semiclassical model for reaction rate constants. J Chem Phys 61:1823–1834. doi:10.1063/1.1682181
56. Yang W, Mortier WJ (1986) The use of global and local molecular parameters for the analysis of the gas-phase basicity of amines. J Am Chem Soc 108:5708–5711. doi:10.1021/ja00279a008
57. Bultinck P, Fias S, Van Alsenoy C, et al (2007) Critical thoughts on computing atom condensed Fukui functions. J Chem Phys 127:34102. doi:10.1063/1.2749518
58. Parr RG, Yang W (1984) Density functional approach to the frontier-electron theory of chemical reactivity. J Am Chem Soc 106:4049–4050. doi:10.1021/ja00326a036
59. Ayers PW, Levy M (2000) Perspective on "density functional approach to the frontier-electron theory of chemical reactivity.". Theor Chem Accounts Theory Comput Model Theor Chim Acta 103:353–360. doi:10.1007/s002149900093
60. Morell C, Grand A, Toro-Labbé A (2005) New dual descriptor for chemical reactivity. J Phys Chem A 109:205–212. doi:10.1021/jp046577a
61. Cárdenas C, Rabi N, Ayers PW, et al (2009) Chemical reactivity descriptors for ambiphilic reagents: dual descriptor, local hypersoftness, and electrostatic potential. J Phys Chem A 113:8660–8667. doi:10.1021/jp902792n
62. Ayers PW, Morell C, De Proft F, Geerlings P (2007) Understanding the Woodward–Hoffmann rules by using changes in electron density. Chem - A Eur J 13:8240–8247. doi:10.1002/chem.200700365
63. Geerlings P, Ayers PW, Toro-Labbé A, et al (2012) The Woodward–Hoffmann rules reinterpreted by conceptual density functional theory. Acc Chem Res 45:683–695. doi:10.1021/ar200192t
64. Pearson RG (1987) Recent advances in the concept of hard and soft acids and bases. J Chem Educ 64:561. doi:10.1021/ed064p561
65. Parr RG, Chattaraj PK (1991) Principle of maximum hardness. J Am Chem Soc 113:1854–1855. doi:10.1021/ja00005a072
66. Ayers PW, Parr RG (2000) Variational principles for describing chemical reactions: the Fukui function and chemical hardness revisited. J Am Chem Soc 122:2010–2018. doi:10.1021/ja9924039
67. Pearson RG, Palke WE (1992) Support for a principle of maximum hardness. J Phys Chem 96:3283–3285. doi:10.1021/j100187a020
68. Torrent-Sucarrat M, Luis JM, Duran M, Solà M (2002) Are the maximum hardness and minimum polarizability principles always obeyed in nontotally symmetric vibrations? J Chem Phys 117:10561–10570. doi:10.1063/1.1517990
69. Torrent-Sucarrat M, Luis JM, Duran M, Solà M (2001) On the validity of the maximum hardness and minimum polarizability

principles for non-totally symmetric vibrations. J Am Chem Soc 123:7951–7952. doi:10.1021/JA015737I

70. Elfström LT, Widersten M (2005) Catalysis of potato epoxide hydrolase, StEH1. Biochem J 390:633–640. doi:10.1042/BJ20050526
71. Tzeng HF, Laughlin LT, Armstrong RN (1998) Semifunctional site-specific mutants affecting the hydrolytic half- reaction of microsomal epoxide hydrolase. Biochemistry 37:2905–2911. doi:10.1021/bi9727388
72. Morisseau C, Beetham JK, Pinot F, et al (2000) Cress and potato soluble epoxide hydrolases: purification, biochemical characterization, and comparison to mammalian enzymes. Arch Biochem Biophys 378:321–332. doi:10.1006/abbi.2000.1810
73. Laidler KJ, King MC (1983) Development of transition-state theory. J Phys Chem 87:2657–2664. doi:10.1021/j100238a002
74. Thomaeus A, Carlsson J, Aqvist J, Widersten M (2007) Active site of epoxide hydrolases revisited: a noncanonical residue in potato StEH1 promotes both formation and breakdown of the alkylenzyme intermediate. Biochemistry 46:2466–2479. doi:10.1021/bi062052s
75. Yamada T, Morisseau C, Maxwell JE, et al (2000) Biochemical evidence for the involvement of tyrosine in epoxide activation during the catalytic cycle of epoxide hydrolase. J Biol Chem 275:23082–23088. doi:10.1074/jbc.M001464200
76. Arand M, Wagner H, Oesch F (1996) Asp333, Asp495, and His523 form the catalytic triad of rat soluble epoxide hydrolase. J Biol Chem 271:4223–4229. doi:10.1074/jbc.271.8.4223
77. Blée E, Summerer S, Flenet M, et al (2005) Soybean epoxide hydrolase: identification of the catalytic residues and probing of the reaction mechanism with secondary kinetic isotope effects. J Biol Chem 280:6479–6487. doi:10.1074/jbc.M411366200